Journal of Materials Chemistry A

Accepted Manuscript

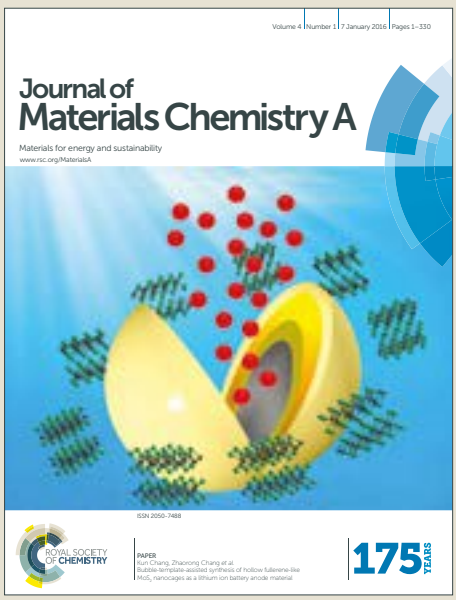

ROYAL SOCIETY OF CHEMISTRY

rsc.li/materials-a

View Article Online
DOI: 10.1039/C9TA00573K

Journal Name

ARTICLE TYPE

Cite this: DOI: 10.1039/xxxxxxxxxx

Electronic properties of heterogenized Ru(II) polypyridyl photoredox complexes on covalent triazine frameworks†

Arthur De Vos,[a] Kurt Lejaeghere,[a] Francesco Muniz Miranda[a], Christian V. Stevens,[b] Pascal Van Der Voort[c] and Veronique Van Speybroeck[a]

Received Date
Accepted Date

DOI: 10.1039/xxxxxxxxxx

www.rsc.org/journalname

Ru(II) polypyridyl complexes have been successful for a wide range of photoredox applications thanks to their efficient light-induced metal-to-ligand charge transfer. Using the computational framework of density-functional theory, we report how these complexes can be anchored onto covalent triazine frameworks while maintaining their favorable electronic properties. We moreover show that variation of the nitrogen content of the framework linkers or complex ligands endows the heterogenized catalyst with a unique versatility, spanning a wide range of absorption characteristics and redox potentials. By judiciously choosing the catalyst building blocks, it is even possible to selectively guide the charge transfer toward either the scaffold or the accessible pore sites. Rational design of sustainable and efficient photocatalysts thus comes within reach.

1 Introduction

To sustain a growing global population, a more efficient and environmentally friendly harvesting of energy is required. This is especially important for the chemical industry, which is one of the most energy-intensive sectors, strongly relying on fossil fuels for the production of chemical products.[1] Photocatalysis is a more sustainable approach, as it relies on naturally present sun light in combination with photocatalytic materials to transfer solar into chemical energy.[2–5] This transfer can be efficiently achieved by homogeneous photocatalysis with the aid of photocatalytic complexes.[3,6] However, as most promising photocatalysts contain precious metals, it is highly desirable to develop recyclable and reusable heterogeneous photocatalytic systems. The use of photocatalytic complexes in a homogeneous suspension necessitates an environmentally unfriendly cycle to remove the catalyst from the products. Heterogeneous catalysts in which the photocatalytic complexes are anchored on a porous framework can avoid this last step and therefore serve as an environmentally cleaner alternative.[7–10] In this work, we not only demonstrate how covalent triazine frameworks (CTFs) provide such a support for photocatalytic Ru complexes, but show that they introduce an additional possibility for tuning the electronic response — and hence efficiency — of the combined photocatalytic system.

The photocatalytic complexes of interest consist of a Ru^{2+} ion octahedrally chelated by three bidentate polypyridyl ligands L, denoted as $Ru(II)L_3$ (see Fig. 1). The photoactivity of these complexes is caused by their long-lived metal-to-ligand charge transfer (MLCT) state induced by light absorption.[3] This MLCT and resulting availability of the excited electron on the ligands enables its good performance as catalytic center, where it triggers oxidation or reduction reactions in surrounding systems.[3,11–17] Proven photoredox applications include carbon dioxide reduction,[18,19] solar cell development,[20] water splitting,[2,21–23] as well as Diels-Alder cycloadditions.[24]

In this paper we consider the heterogenization of these $Ru(II)L_3$ complexes onto covalent triazine frameworks using a computational approach. CTFs are part of a much broader family of porous frameworks suitable for anchoring photocatalytic complexes. This family includes metal-organic frameworks (MOFs)[25] and covalent-organic frameworks (COFs),[26–28] many of which have the high surface areas mandatory to function as a good support material. Moreover MOFs and COFs are highly tunable due to the variability of their building blocks, adding a second pathway to modify the material in addition to the anchored complex. Such alternative modification strategies are ideal to engineer electronic and

[a] Center for Molecular Modeling (CMM), Ghent University, Technologiepark 46, 9052 Zwijnaarde, Belgium. E-mail: Kurt.Lejaeghere@UGent.be, Veronique.VanSpeybroeck@UGent.be
[b] Research Group SynBioC, Department of Green Chemistry and Technology, Faculty of Bioscience Engineering, Ghent University, Campus Coupure, Coupure Links 653 bl. B, 9000 Gent, Belgium
[c] Center for Ordered Materials, Organometallics and Catalysis (COMOC), Department of Inorganic and Physical Chemistry, Ghent University, Krijgslaan 281 (S3), 9000 Gent, Belgium

† Electronic Supplementary Information (ESI) available. See DOI: 10.1039/b000000x/

View Article Online
DOI: 10.1039/C9TA00573K

optical behaviour.[29,30] Unfortunately, most MOF structures tend to lack stability under reaction conditions.[13,31,32] COFs, on the other hand, are more stable, and even display some (photo)catalytic activity in their pristine form,[33–38] although they lack an inorganic catalytic center compared to MOFs. Using COFs as a support for photocatalytic complexes may lead toward more efficient and robust heterogeneous photocatalysis.

CTFs are an especially promising class of COFs known to be thermally and chemically stable.[35,39–42] They are 2D porous frameworks made upon the trimerization of aromatic nitriles. CTFs are particularly interesting to anchor photocatalytic complexes, as they are much lighter than most other porous materials and do not possess toxic or environmentally unfriendly elements. In addition, 2D heterostructures have attracted widespread attention thanks to their compelling properties, which are useful for many potential applications.[43]

In order to use CTFs as support material, bidentate nitrogen-containing linkers similar to the chelating ligands of the Ru(II)L_3 complex should be present in the framework. We start from a biphenyl-based CTF,[44] which we will refer to as CTF-1-2R[45] (the name CTF-2, which has also been used for this material[44] was originally proposed for a naphthalene-based structure[46]). Note that CTF-1-2R intrinsically has some photocatalytic activity.[44] We then replace a number of biphenyl linkers with polypyridyl ones suited to anchor the Ru(II)L_3 complex (see Figure 1). Hug et al. recently synthesized such a CTF-1-2R containing a 2-2'-bipyridine (bipy) linker.[47] Similar strategies can be applied for MOFs,[48] where photocatalytic complexes were already successfully anchored to both linkers[49,50] and nodes.[51]

In the following sections, we perform a computational investigation of the combined Ru(II)L_3-CTF heterogeneous photocatalyst and explore in how far the favorable electronic properties of Ru(II)L_3 complexes are maintained upon anchoring. To investigate this point, we vary the bidentate moieties in both the Ru(II)L_3 complex and the CTF support and show how small synthetic modifications allow tuning the light absorption and redox properties of the catalyst. The CTF and the Ru(II)L_3 complex are first considered separately, after which the properties of the coupled catalyst are compared in detail. The combined Ru(II)L_3-CTF heterogeneous photocatalyst has a larger versatility than the isolated complex as both the framework and the Ru(II)L_3 complex can be varied. In addition, it makes it possible to obtain asymmetrically surrounded Ru(II)L_3 complexes in a rather natural way. We show that depending on the composition of the system the MLCT can be guided[52] either to the framework or to the pore of the material, producing a versatile photocatalyst for either interface- or pore-driven catalytic applications.

2 Methodology

2.1 Structures

We considered several variants of the CTF-1-2R framework to act as a scaffold for Ru(II)L_3 complexes. CTF-1-2R itself only contains biphenyl linkers (biph) and is therefore unsuited to function as a catalytic support for the photocatalytic Ru(II)L_3 complex. To introduce appropriate anchor sites, four experimentally available bidentate nitrogen-containing linkers were instead considered, cis-bipyridine (cbipy), phenanthroline (phen), cis-bipyrazine (cbipz), and bipyrimidine (bipm), as well as their monodentate trans configurations (tbipy, tbipz) (see Figure 1). This set of linkers allows changing the nitrogen content of the CTF's aromatic system, with nitrogen counts ranging from two to four per linker. Moreover, experimental synthesis of these materials should be possible, as demonstrated by the successful synthesis of a bipyridine-based CTF by Hug *et al.*[47]

We modeled the nitrogen-containing CTFs by considering a single CTF-1-2R monolayer, which contains three biph linkers and two triazine (tria) secondary building blocks (SBU) per unit cell. The influence of multilayer stacking is therefore not taken into account. In each layer we replaced one, two or three of the biph linkers by a particular polypyridyl one (L^i), forming a modified CTF-1-2R. We will refer to a given CTF in terms of its constituent linkers, e.g. $biph_3$ for CTF-1-2R and $L^i_n biph_{3-n}$ for the modified systems with n the number of replaced biph linkers. The systematic and controlled inclusion of polypyridyl linkers within the CTF allows us to assess the influence of nitrogen content on the CTF properties. The work of Wang *et al.* moreover indicates that it is indeed possible to make such mixed-linker CTFs.[53]

The properties of the Ru(II)L_3 complex were varied using the same four bidentate ligands. Ru(II)L_3 complexes used for homogeneous photocatalysis consist of three bidentate nitrogen-containing ligands for which generally two or three are equal.[3,12–15] We will denote these complexes as Ru(II)$L^j_2 L^i_1$, with the most prominent example being Ru(II)$cbipy_3$. When embedded into the CTF, the L^i linker is shared between the framework and the complex, while the other two chelating ligands L^j extend into the pore. Such metal-functionalized COFs may be produced either post-synthetically or by using prefunctionalized linkers during the CTF synthesis.[13,54] We denote the resulting heterogenized photocatalyst as (Ru(II)L^j_2)L^i_1($L^i_n biph_{2-n}$) with $n = 0, 1, 2$. The presence of mixed-ligand complexes rather than complexes with only a single type of ligand allows us to tune the photocatalytic activity in much more detail.

2.2 Computational Details

All periodic calculations were performed using density-functional theory (DFT) in the projector-augmented wave (PAW) approach[55] with the VASP 5.4.4 package[56–59] and employing the PBE functional.[60] Although the semilocal PBE functional substantially underestimates band gaps, it correctly reproduces electronic-structure trends at a fraction of the cost of higher-level methods.[29,45,61] We confirmed this using selected HSE06 calculations (see Figure S2-S5†).[62,63] Note, however, that for quantitative purposes, even more advanced theories would be required, as conjugated systems typically yield poor absolute electron affinity and band gap predictions.[64] Van der Waals interactions were modeled by the DFT-D3 method of Grimme with Becke-Jonson damping.[65,66] The recommended GW-ready PAW potentials were used because of their high precision,[67,68] employing a $1s^1$, $2s^2\,2p^2$, $2s^2\,2p^3$ and $4s^2\,4p^6\,5s^2\,4d^6$ valence electron configuration for respectively H, C, N and Ru. In addition, a plane wave basis set was employed

View Article Online
DOI: 10.1039/C9TA00573K

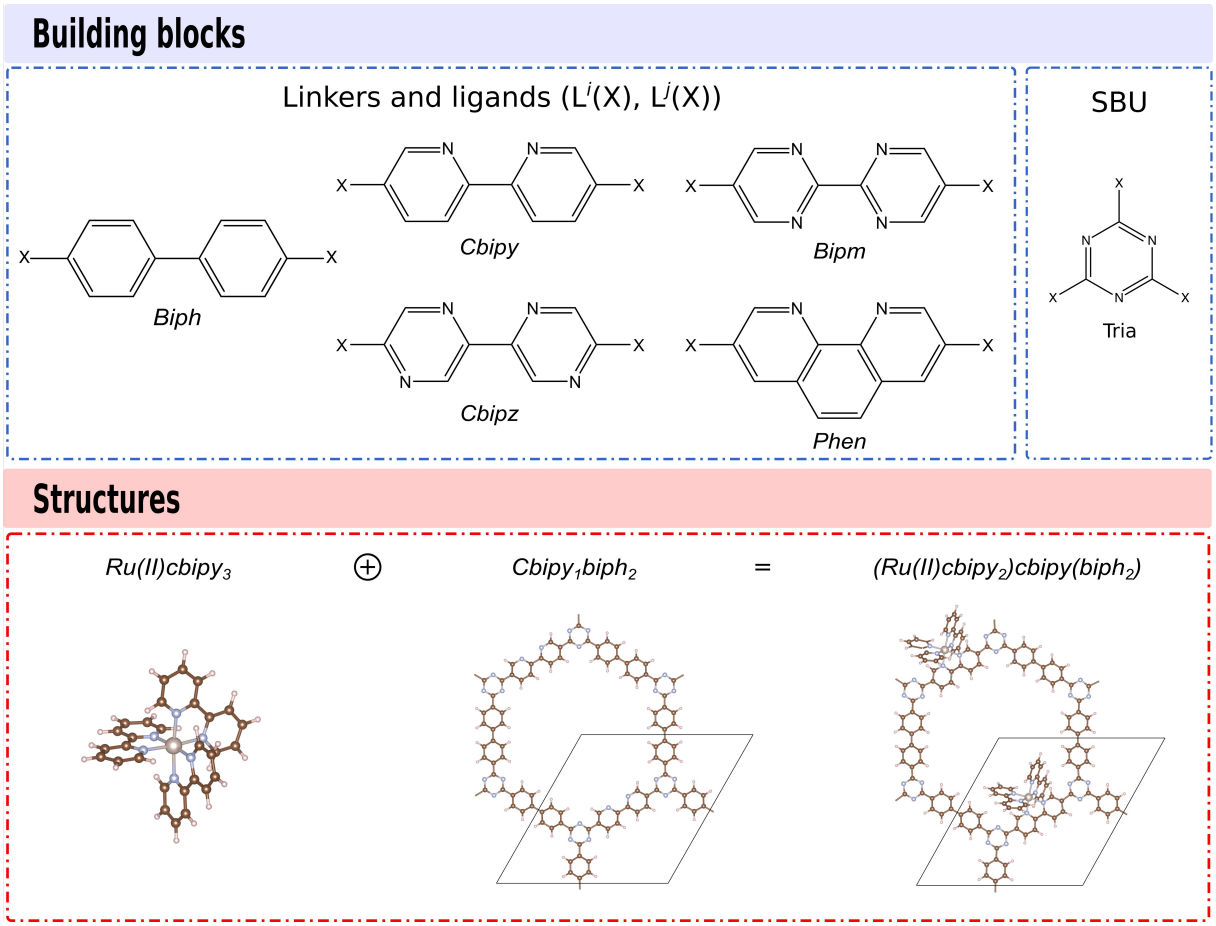

Fig. 1 Building blocks of both the CTF monolayer and the Ru(II)L_3 complexes (top). The heterogeneous photocatalyst of interest consists of a structure in which the Ru(II)L_3 complex is anchored on a CTF monolayer, for which an example is given (bottom) (blue: N, brown: C, white: H, grey: Ru).

with a kinetic energy cut-off of 800 eV for all structures.

For CTF monolayers a $2 \times 2 \times 1$ Γ-centered grid was used to sample the first Brillouin zone. We imposed an electronic energy convergence criterion of 10^{-5} eV together with an ionic relaxation threshold of 10^{-4} eV. These settings were used to uniformly rescale the CTF's in-plane lattice parameters from −4% to 4% in steps of 1% and fit a Rose-Vinet equation of state (see e.g. Figure S8†).[69] Because of the intrinsic periodicity imposed by VASP, an interlayer distance of 22 Å was maintained, and the van der Waals radius in the D3 scheme was reduced to 20 Å to remove dispersion interaction between the monolayers. The equilibrium lattice parameters were extracted from the equation of state, at which the structures were relaxed using more stringent electronic and ionic convergence criteria of 10^{-7} eV and 10^{-6} eV, respectively. In this last optimization run, the interlayer vacuum region was increased to 40 Å when a Ru(II)L_3 complex was anchored onto the CTF to obtain reliable energies.

The Ru(II)L_3 complexes were calculated in a $40 \times 40 \times 40$ Å^3 unit cell using a 2+ charge, a Γ-point *k*-grid and an electronic and ionic convergence threshold of 10^{-7} eV and 10^{-6} eV. Similarly, the Ru^{2+} ion and nitrogen-containing linkers were calculated in a $20 \times 21 \times 23$ Å^3 and $40 \times 30 \times 22$ Å^3 box (see Figure S6†) to obtain the formation energy (see "The photocatalytic complex" and "The heterogeneous photocatalyst"). In the case of a charged system, an energy correction was applied to remove monopolar interactions with its periodic images (see Section S2†).[68,70,71]

Density of states (DOS) calculations were performed with a $6 \times 6 \times 1$ Γ-centered grid for the CTF and a Γ-point grid for the building blocks and Ru(II)L_3 complexes. In addition, the threshold for the electronic self-consistent cycle was tightened to 10^{-8} eV. The DOS were plotted using the pymatgen package.[72] Depending on the feature of interest, different DOS plots were aligned using either a judiciously chosen energy or potential reference, or by quantitatively positioning them with respect to the vacuum potential. In the latter case, the vacuum potential was either explicitly calculated (neutral systems) or determined from the electron affinity, i.e. the energy change upon adding a supplementary electron (charged systems).

3 The scaffold

To understand the role of the CTF scaffold's composition in the heterogeneous photocatalyst, we first consider the CTF alone. We examine both the energetic and the electronic influence of introducing polypyridyl linkers within the $biph_3$ monolayer, which are needed to create a suitable anchor site for the Ru(II)L_3 complex (see "Structures").

View Article Online
DOI: 10.1039/C9TA00573K

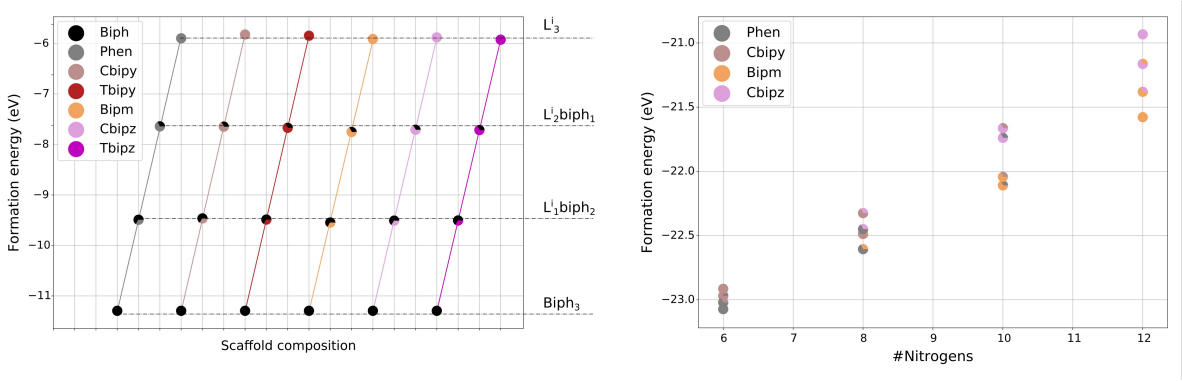

(a) CTF **(b)** $Ru(II)L_3$

Fig. 2 Formation energy of the CTF scaffold (a) and the $Ru(II)L_3$ complex (b) in eV per unit cell. Each data point is colored in three parts, which represent the composition of the CTF scaffold or $Ru(II)L_3$ complex, respectively. In panel (a) the solid lines connect all frameworks $L^i_n biph_{3-n}$ with a fixed linker type L^i; the dashed lines correspond to different values of n.

Energetics. As CTFs are made upon trimerisation of aromatic nitriles (see Figure 1, X=CN), the CTF stability can be assessed by evaluating the formation energy in terms of these constituting linkers (see Table S5†):

$$E_{Form} = E_{\mathrm{CTF}} - \sum_i E_{\mathrm{L}^i(\mathrm{CN})} = \sum_i \Delta E_{\mathrm{L}^i(\mathrm{CN})} \quad (1)$$

The formation energy is depicted in Figure 2a. We see that all frameworks are stable, but that the stability scales unfavorably with the number of polypyridyl linkers. This destabilization per linker is of the order of 1.8 eV and is approximately equal for all linkers within a 40 meV range, independent of their nitrogen content.

To investigate the role of the individual linkers in more detail, Eq. 1 can be approximated to attribute the formation energy to independent contributions of the different linkers. In this case, the formation energy can be seen as the sum of stabilization energies $\Delta E_{\mathrm{L}^i}(\mathrm{CN})$ per linker, independent of the framework in which they are incorporated. These stabilization energies per linker can be obtained from the formation energies of different CTFs via a least-squares fit (see Table S6†. The agreement between the actual and the fitted formation energies is better than 3 meV, indicating that there is no energetic interaction between individual linkers across the bridging triazine unit.

Electronic structure. The densities of states for a few considered CTFs are shown in the right panel of Figure 3 (see Section S5.2† for a full overview and Figure S2† for a HSE06 validation of Figure 3). The decomposition with respect to the building blocks shows the appearance of both localized and delocalized states. The delocalized states, which include the conduction band minimum (CBM), are spread out over the entire structure and agree well with the traditional solid-state concept of an energy band. In contrast, there are also localized states, such as the top of the valence band, which are characterized by sharp peaks in the DOS. The corresponding orbitals are confined to individual components of the CTF and retain a more discrete, molecular character.[29,73,74] These localized states are therefore often referred to as crystal orbitals, and the top of the valence band is classified as highest occupied crystal orbital (HOCO). Strikingly, the energy and shape of these localized electron levels is very similar to those in the CTF constituents (see Figure 3, left panel). This suggests that some features of the linkers are maintained when incorporating them into the aromatic system of the periodic CTF. Such electronic structure decoupling resembles that of 0D MOFs, which are made up of independent contributions of their inorganic and organic building blocks.[29,61] Hence we would like to introduce the idea of orthogonal electronic structure engineering for COFs in a similar way as for MOFs, i.e. the ability to tune the overall electronic structure by independently varying the different constituents.

Finally Figure 3 illustrates that the electronic structure of CTF-1-2R can be modified by doping it with nitrogen-containing linkers. Although the position of the HOCO relative to the vacuum energy remains fairly independent of the nitrogenous character of the framework, the CBM systematically lowers if it is increased (see Figure 3 and Figure S9†). As a result the band gap decreases. The band gap is plotted for the various materials in terms of the nitrogen content in Figure 4a. The behavior of the CBM is found to be inherited from the individual linkers (see Section S4†) and is in line with current literature on similar nitrogen-based organic frameworks.[34,75,76] It is caused by the inclusion of nitrogen atoms in the aromatic ring. Because their free electron pairs are not part of the aromatic system, they lead to a π-electron-deficient system. The framework (or linker) will therefore accept electrons more easily. The resulting band gap may be more suitable for photocatalysis, as experimentally observed in nonfunctionalized CTFs.[34,36,37,44,46,76] In addition, the dependence of the band gap on nitrogen content may be relevant during photocatalysis as it could favor the transport of excited electrons from the photocatalytic complex to the framework (see "The heterogeneous photocatalyst")

View Article Online
DOI: 10.1039/C9TA00573K

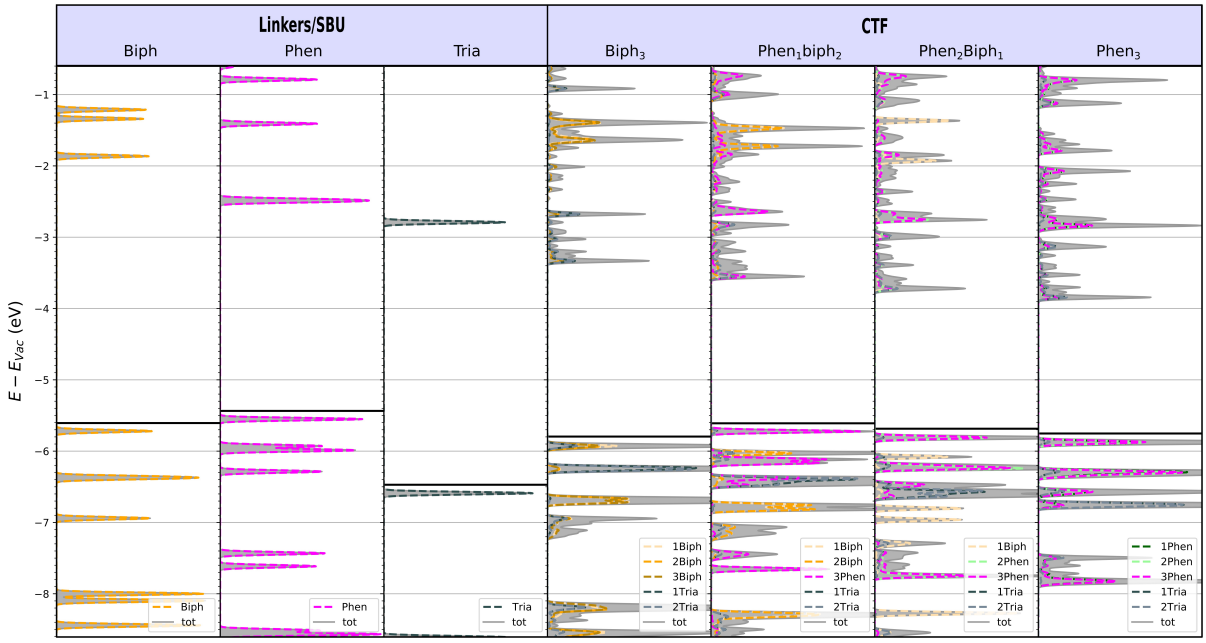

Fig. 3 Densities of states of CTF-1-2R doped with 1, 2 or 3 phenanthroline linkers ($\text{phen}_n\text{biph}_{3-n}, n = 0, 1, 2, 3$) compared to the electronic structure of the hydrogen-terminated constituents (biph, phen, tria). The DOS are aligned with respect to the vacuum energy.

4 The photocatalytic complex

Essential to the photocatalytic performance of the envisioned heterogeneous photocatalyst is the activity of the Ru(II)L_3 complex. Similar to the CTF scaffold, several nitrogen-containing ligands can be considered to further tune the properties of this complex. Here we investigate the energetics and electronic properties of mixed-ligand Ru(II)L_3 complexes with up to two different polypyridyl moieties (see "Structures").

Energetics. Ru(II)L_3 complexes are a combination of a Ru^{2+} ion and nitrogenous bidentate ligands (see Figure 1 with X=H). Their stability can therefore be calculated from the following formation energy (see Table S8†):

$$E_{Form} = E_{\text{RuL}_3^{2+}} - \sum_j E_{\text{L}^j(\text{H})} - E_{\text{Ru}^{2+}} = \sum_j \Delta E_{\text{L}^j(\text{H})} \qquad (2)$$

Note that by using Eq. 2 competition with other ligands is not considered. However, the latter stability is corroborated by the confirmed functionality of Ru(II) complexes in several photocatalytic reactions.[2,3,11–24]

The energy can again be successfully decomposed into contributions from the different ligands with a residual error of less than 4 meV ($\Delta E_{\text{L}^j(\text{H})}$, see Table S9†). This implies that there is little energetic coupling between the different ligands across the Ru ion, so the main differences between Ru(II)L_3 complexes can be attributed to the Ru(II)-L^j bonds.

The experimentally observed stability of Ru(II)L_3 complexes is confirmed in our calculations (see Figure 2b). Moreover, we note that ligands with few nitrogen atoms bind more strongly into a Ru(II)L_3 complex, which is in line with their larger basicity and associated stronger electron-donating character. This simple criterion suggests that a Ru(II)L_3 complex might be post-synthetically applied to an existing CTF crystal when the complex ligands have a higher nitrogen content than the framework linkers. In this way the Ru(II)L_3 complex would anchor more strongly to the framework and exchange one of its ligands for a framework linker. We investigate this conjecture in more detail in "The heterogeneous photocatalyst".

Electronic structure. The highest occupied molecular orbital (HOMO) of Ru(II)L_3 complexes is centered on the Ru^{2+} ion and corresponds to a t_{2g} state of an octahedrally surrounded complex. The lowest unoccupied molecular orbital (LUMO), on the other hand, is located on the chelating ligands with the highest nitrogen content and thus highest electron affinity (see Figure 5 or Section S6.2† for a full overview and Figure S4† for a HSE06 validation of Figure 5). The HOMO-LUMO gap therefore represents a qualitative measure of the MLCT, which is one of the key properties in the photocatalytic process of interest. The nitrogen dependence of the LUMO location moreover allows tuning the MLCT to a specific ligand, which is of interest when anchoring the complex to a CTF. This larger reduction potential of Ru(II)L_3 complexes with increasing nitrogen content was also observed experimentally.[3]

Similar to CTFs, the electronic structure of a Ru(II)L_3 complex can to a large extent be considered as a superposition of contributions of its components (see Figure S10†). Therefore, even here the concept of orthogonal electronic structure engineering can be introduced. As the Ru(II)L_3 complex contains the same type of linkers/ligands as the CTF, its electronic structure moreover evolves in a similar way as a function of nitrogen content. Indeed, the lowest unoccupied linker state lowers as the nitrogen content increases, while the highest occupied linker state remains rather constant. This leads to an overall decrease of the ligand-

View Article Online
DOI: 10.1039/C9TA00573K

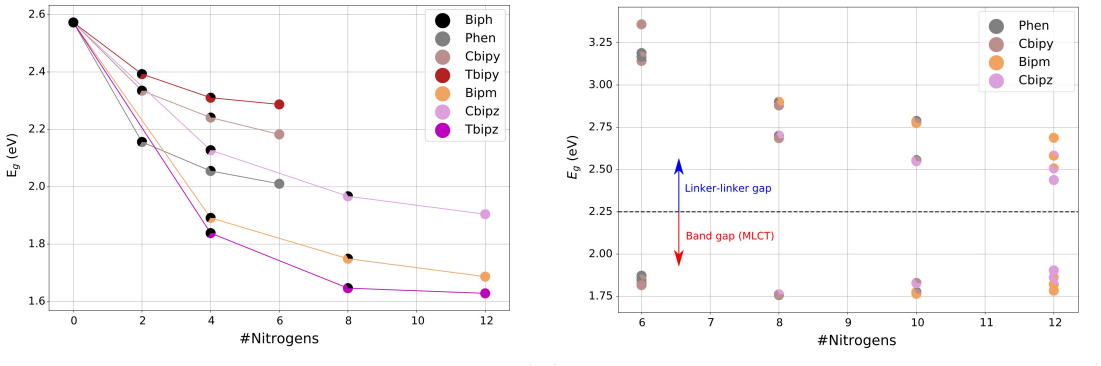

(a) CTF **(b)** Ru(II)L_3

Fig. 4 Band gap of the CTF as a function of the number of linker nitrogen atoms per unit cell (a). Gap between the highest occupied and lowest unoccupied molecular orbital and analogous linker-linker gap of the Ru(II)L_3 complex with respect to the number of nitrogen atoms in the complex (b). Each data point is colored in three parts, which represent the composition of the CTF scaffold or Ru(II)L_3 complex, respectively.

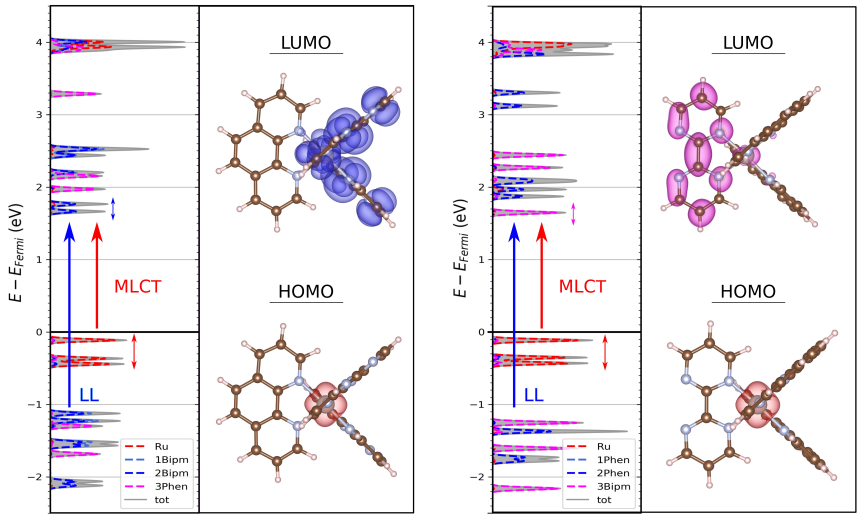

(a) Ru(II)bipm$_2$phen$_1$ **(b)** Ru(II)phen$_2$bipm$_1$

Fig. 5 Metal-to-ligand (MLCT) and ligand-ligand (LL) transitions in Ru(II)bipm$_2$phen$_1$ (a) and Ru(II)phen$_2$bipm$_1$ (b) together with the corresponding orbitals.

ligand (LL) gap with increasing nitrogen content (see Figure 4b and Figure 5). On the other hand, the HOMO is now a Ru-based state and lowers as much in energy with nitrogen content as the LUMO. As shown in Figure 4b, this gives rise to a fairly constant HOMO-LUMO gap. Hence, the absorption behaviour is similar across the different mixed Ru(II)L_3 complexes, although the redox potential is changing. This feature makes our Ru(II)L_3 complexes an interesting set for photocatalysis as it allows adapting both the direction of the MLCT and the chemical activity while targeting the same range of absorption wavelengths.

5 The heterogeneous photocatalyst

Both the CTF scaffold and the homogeneous Ru(II)L_3 catalyst display interesting properties for photocatalytic purposes. They can be combined in numerous ways, which enables fine-tuning the material beyond what is possible in the individual constituents. However, it is not guaranteed that the beneficial behaviour of the components is transferred to the combined Ru(II)L_3-CTF system. We consider the energetics and electronic properties of a systematic subset of heterogeneous photocatalysts below (see Table S1†). Not only does this demonstrate that the photocatalytic properties of both the complex and the framework are maintained, but they can even be varied with an unparalleled versatility, allowing different phototransfer directions and redox potentials.

Energetics. Similar to the treatment of the CTF scaffold or the Ru(II)L_3 complex, the formation energy of the Ru(II)L_3-CTF catalyst can be calculated with respect to the individual constituents (see Table S11†). We find the same trends in stability when we vary the components of either the Ru(II)L_3 complex or the CTF (see Figure S12†). Incorporating nitrogenous linkers in either

View Article Online
DOI: 10.1039/C9TA00573K

part not only destabilizes the material, but by approximately the same amount as in the separate building blocks (see Table S12†). The energetics of the combined Ru(II)L_3-CTF catalyst can therefore be predicted to some extent from this underlying behavior.

Of particular interest to the combined Ru(II)L_3-CTF catalyst is the energy required or released when anchoring the photocatalytic complex onto the support framework. We calculated the energy needed to anchor a Ru(II)L_3^j complex with three equal ligands onto a $L^i_{n+1}biph_{2-n}$ CTF to form the anchored $(Ru(II)L_2^j)L_1^i(L_n^i biph_{2-n})$ complex ($n = 0, 1, 2$). For all considered catalysts this energy was found to be negative (see Table S13†), indicating that the heterogeneous photocatalyst can indeed be formed through a spontaneous process of ligand exchange. Moreover highly nitrogen-containing Ru(II)L_3^j complexes anchor more strongly to CTFs with a lower nitrogen content, which possess a higher basicity. This is in correspondence with the energetics of the isolated Ru(II)L_3 complex.

Electronic structure. Ru(II)L_3 complexes combine a band gap in the visible wavelength range with an intrinsic charge transfer upon light absorption. The combined Ru(II)L_3-CTF catalyst will only be successfully created if these advantages remain intact. A first requirement is that the electronic structure of the complex within the catalyst should not differ too much from that of the isolated one. Figure 6a illustrates that the energy levels of the pristine Ru(II)bipm$_2$phen complex (left panel) are indeed retrieved when anchoring it onto a phenanthroline-containing framework (right panel) (see Figure S14-S15† for further examples and Figure S5a† for an HSE06 validation of Figure 6a). Furthermore the redox potential of the complex remains almost unaltered, indicating that the heterogeneous photocatalyst may be applied to the same reactions as the homogeneous one. The principle of orthogonal electronic structure engineering therefore also extends to the combined Ru(II)L_3-CTF catalyst, in which not only states of the Ru(II)L_3 complex, but also from the CTF are recovered (see Figure S13†).

A second point of attention is the electronic structure near the band gap. We showed in "The photocatalytic complex" that the Ru(II)L_3 complex has a Ru-centered HOMO and a ligand-based LUMO. When anchored, the HOCO moves toward a non-anchoring CTF linker state (see Figure 6). Excitations from this level may be of interest, but it is spatially separated from the Ru^{2+} ion. Further study is therefore needed to elucidate whether transitions between such a framework linker and the Ru(II)L_3 complex are realistic. We instead focus on MLCT excitations of the anchored Ru(II)L_3 separately, which we find to display the same trends as the Ru(II)L_3 complex. Indeed the LUCO and the Ru levels again decrease as a function of the nitrogen content of the Ru ligands while the highest occupied ligand states remain more or less fixed (see Fig S14†). As a result, the MLCT gap remains independent of the used ligands, while the LL gap decreases with nitrogen content. These findings suggest a Ru(II)L_3 complex to retain its photoredox properties when it is heterogenized in the CTF. The heterogenized photocatalyst may therefore be suited for similar reactions as the isolated complex.

Although the general electronic properties of the Ru(II)L_3 complex are conserved, heterogenizing the Ru(II)L_3 complex onto the CTF does have some interesting consequences. The most prominent effect is the introduction of a CTF-centered HOCO, as mentioned above. A second result is visible for the unoccupied states (Figure 6a). Not only is the electron affinity increased as a function of the CTF nitrogen content, but this affects the anchoring linker differently from the ones dangling into the pore. It may even lead to a change in energy ordering between the different unoccupied ligand orbitals (see Figures. S15b, c†). In that case, an MLCT-excited electron from the Ru(II)L_3 complex may change its charge transfer direction compared to the isolated cluster, i.e. toward the framework rather than the other two (pore) ligands.

Attaching the Ru(II)L_3 complex to a CTF does not appear to undermine its photoactivity nor the redox reactions to which it is applied. On the contrary, modifying the CTF linkers provides an additional degree of freedom to tune the electronic response of the photocatalyst. By varying the polypyridyl linkers in the CTF or the corresponding ligands in the Ru(II)L_3 complex, the redox potential of the catalyst can be altered by up to 1 eV. This versatility is useful to further optimize Ru(II)L_3 complexes for sustainable applications, such as water splitting[23] and carbon dioxide reduction.[19] Such design may be accomplished using the qualitative guidelines established here, as well as by means of future investigations into quantitative redox potentials, e.g. by including the solvent and applying a higher level of theory. In addition, carefully selecting both the complex and CTF components allows the design of a guided metal-to-ligand charge transfer (see Figure 6b). In a mixed Ru(II)L_3 complex the MLCT is directed toward the ligand with the highest nitrogen content. When combined with the CTF, a higher nitrogen content of the framework favors a MLCT toward the anchoring linker. If the catalytic operation requires excitation to the framework, the nitrogen content should therefore be high in the CTF and low for the ligands in the pore (e.g. (Ru(II)cbipy$_2$)bipm(bipm$_2$)). In contrast, MLCT toward the pore can be achieved by keeping the nitrogen content of the framework at a minimum and using highly nitrogenous moieties for the pore linkers (e.g. (Ru(II)bipm$_2$)phen(phen$_2$)). This is also the energetically most favored scenario (see Table S13†).

6 Conclusion

Heterogenization of Ru polypyridyl complexes is an essential step in the development of more sustainable photoredox catalysts. A promising possibility in that respect is attaching the complexes to covalent triazine frameworks, which provide a robust and lightweight support. The composition of these 2D porous substrates may moreover be tuned to the redox reaction of interest. CTF-anchored complexes therefore not only offer a large accessible surface, but also a promising versatility toward functional catalyst design.

We considered a wide range of different polypyridyl-based CTF monolayers and Ru(II)L_3 complexes and demonstrated that it is indeed energetically favorable to anchor the Ru complexes onto the CTF. However, an essential condition for an efficient heterogeneous photocatalyst is that its photoredox properties do not deteriorate when incorporated into the CTF scaffold. We confirmed that the electronic structure of both the Ru(II)L_3 complex and CTF

View Article Online
DOI: 10.1039/C9TA00573K

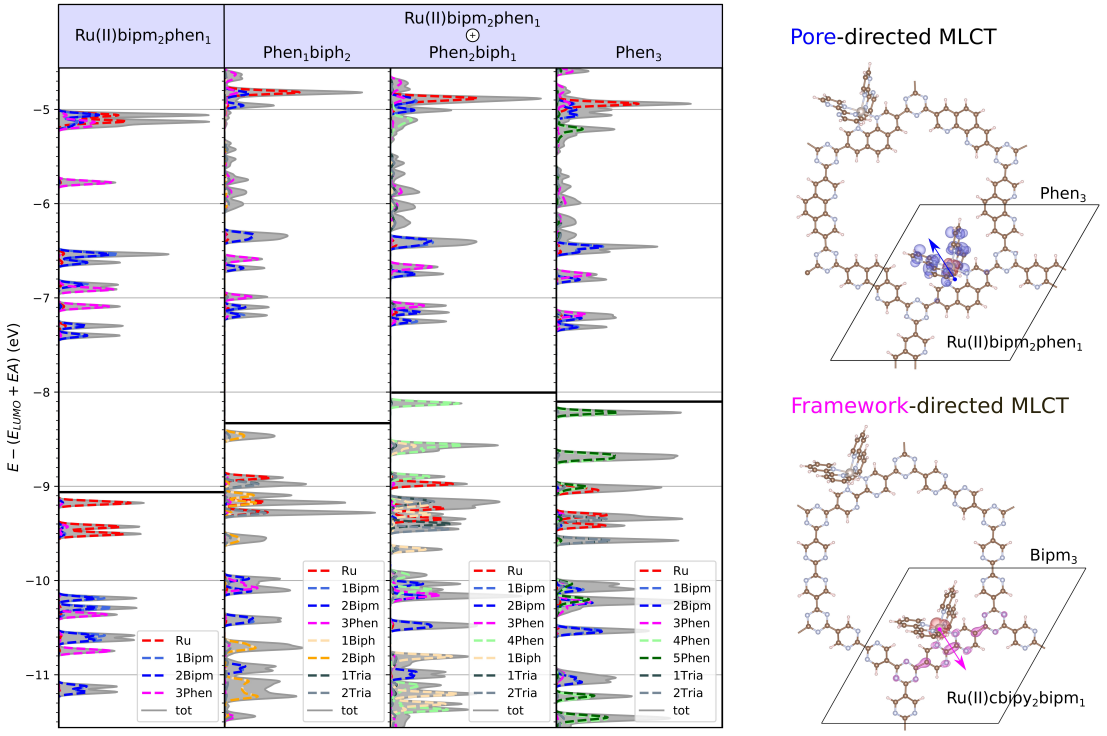

Fig. 6 Electronic states of the Ru(II)bipm$_2$phen$_1$ complex in vacuo and when anchored on a phen$_n$biph$_{3-n}$, $n = 1, 2, 3$ framework (left). Depending on the Ru(II)L$_3$ complex and CTF scaffold, the charge transfer upon light absorption can be directed toward the pore or the framework (right).

stay mostly unaltered upon combining the two systems, and that the redox potential of the photocatalytic complex remains largely the same. This behaviour was shown to be even more generally valid: the energy levels of both the unfunctionalized CTF and the Ru(II)L$_3$ complex are to a large extent made up of contributions from their individual components. Also energetically, the stability of a given structure solely depends on the type of linker or ligand that is introduced into the material. This conclusion indicates that the principle of orthogonal electronic structure engineering, first demonstrated for 0D MOFs,[29] might be applicable to a wide class of crystals with molecule-like building blocks.

Although the heterogenization of photocatalytic Ru(II)L$_3$ complexes is a valuable target as such, our study additionally showed that anchoring onto a CTF scaffold provides the system with an even broader tunability than before. Band gaps, charge transfer reactions and redox potentials are all strongly adaptable by changing the nitrogen content of the different components of the catalyst. A higher nitrogen content typically lowers the energy of unoccupied polypyridyl levels and occupied Ru t_{2g} levels, while occupied linker or ligand states change only little. This behavior makes it possible to guide the light-induced charge transfer by increasing the nitrogen content of either the CTF (framework-directed MLCT) or the dangling Ru ligands (pore-directed MLCT). The versatility of CTF-anchored Ru(II)L$_3$ complexes therefore endows them with the capability to display a high photoredox activity for a wide range of target reactions and catalytic set-ups.

Acknowledgements

We acknowledge financial support by the Fund for Scientific Research Flanders (FWO) and the Research Board of Ghent University through a Concerted Research Action (GOA). The computational resources and services used in this work were provided by VSC (Flemish Supercomputer Center), funded by Ghent University, FWO, and the Flemish Government department EWI.

Conflict of Interest

The authors declare no conflict of interest.

Notes and references

1 U.S. International Energy Agency, *International Energy Outlook*, 2016, DOE/EIA-0484(2016).
2 K. Takanabe, *ACS Catal.*, 2017, **7**, 8006–8022.
3 C. K. Prier, D. A. Rankic and D. W. C. MacMillan, *Chem. Rev.*, 2013, **113**, 5322–5363.
4 M. D. Kärkäs, J. A. Porco and C. R. J. Stephenson, *Chem. Rev.*, 2016, **116**, 9683–9747.
5 D. M. Schultz and T. P. Yoon, *Science*, 2014, **343**, 1239176.
6 J. M. R. Narayanam and C. R. J. Stephenson, *Chem. Soc. Rev.*, 2011, **40**, 102–113.
7 A. G. Slater and A. I. Cooper, *Science*, 2015, **348**, aaa8075.
8 S. M. J. Rogge, A. Bavykina, J. Hajek, H. Garcia, A. I. Olivos-Suarez, A. Sepúlveda-Escribano, A. Vimont, G. Clet, P. Bazin, F. Kapteijn, M. Daturi, E. V. Ramos-Fernandez, F. X. Llabrés i Xamena, V. Van Speybroeck and J. Gascon, *Chem. Soc. Rev.*, 2017, **46**, 3134–3184.
9 H. Takeda, M. Ohashi, Y. Goto, T. Ohsuna, T. Tani and S. Inagaki, *Adv. Func. Mater.*, 2016, **26**, 5068–5077.

View Article Online
DOI: 10.1039/C9TA00573K

10 W. Tu, Y. Xu, S. Yin and R. Xu, *Adv. Mater.*, 2018, **30**, 1707582.
11 J. J. Concepcion, J. W. Jurss, M. K. Brennaman, P. G. Hoertz, A. O. T. Patrocinio, N. Y. Murakami Iha, J. L. Templeton and T. J. Meyer, *Acc. Chem. Res.*, 2009, **42**, 1954–1965.
12 J. M. R. Narayanam, J. W. Tucker and C. R. J. Stephenson, *J. Am. Chem. Soc.*, 2009, **131**, 8756–8757.
13 C. Wang, Z. Xie, K. E. deKrafft and W. Lin, *J. Am. Chem. Soc.*, 2011, **133**, 13445–13454.
14 S. Fukuzumi, T. Kishi, H. K., Y.-M. Lee and W. Nam, *Nat. Chem.*, 2010, **3**, 38–41.
15 D. A. Nicewicz and D. W. C. MacMillan, *Science*, 2008, **322**, 77–80.
16 J.-M. Zen, S.-L. Liou, A. S. Kumar and M.-S. Hsia, *Angew. Chem. Int. Ed.*, 2003, **42**, 577–579.
17 W. Chen, F. Rein and R. Rocha, *Angew. Chem. Int. Ed.*, 2009, **48**, 9672–9675.
18 H. Takeda and O. Ishitani, *Coord. Chem. Rev.*, 2010, **254**, 346 – 354.
19 T. J. Meyer, *Acc. Chem. Res.*, 1989, **22**, 163–170.
20 F. Gao, Y. Wang, J. Zhang, D. Shi, M. Wang, R. Humphry-Baker, P. Wang, S. M. Zakeeruddin and M. Grätzel, *Chem. Commun.*, 2008, 2635–2637.
21 J. J. Concepcion, J. W. Jurss, J. L. Templeton and T. J. Meyer, *J. Am. Chem. Soc.*, 2008, **130**, 16462–16463.
22 N. Kaveevivitchai, R. Chitta, R. Zong, M. El Ojaimi and R. P. Thummel, *J. Am. Chem. Soc.*, 2012, **134**, 10721–10724.
23 M. Graetzel, *Acc. Chem. Res.*, 1981, **14**, 376–384.
24 S. Lin, M. A. Ischay, C. G. Fry and T. P. Yoon, *J. Am. Chem. Soc.*, 2011, **133**, 19350–19353.
25 J. R. Long and O. M. Yaghi, *Chem. Soc. Rev.*, 2012, **112**, 673–1268.
26 C. S. Diercks and O. M. Yaghi, *Science*, 2017, **355**, eaal1585.
27 A. P. Côté, A. I. Benin, N. W. Ockwig, M. O'Keeffe, A. J. Matzger and O. M. Yaghi, *Science*, 2005, **310**, 1166–1170.
28 M. S. Lohse and T. Bein, *Adv. Func. Mater.*, 2018, **28**, 1705553.
29 A. De Vos, K. Hendrickx, P. Van Der Voort, V. Van Speybroeck and K. Lejaeghere, *Chem. Mater*, 2017, **29**, 3006–3019.
30 D. D. Medina, M. L. Petrus, A. N. Jumabekov, J. T. Margraf, S. Weinberger, J. M. Rotter, T. Clark and T. Bein, *ACS Nano*, 2017, **11**, 2706–2713.
31 N. C. Burtch, H. Jasuja and K. S. Walton, *Chem. Rev.*, 2014, **114**, 10575–10612.
32 K. Leus, T. Bogaerts, J. De Decker, H. Depauw, K. Hendrickx, H. Vrielinck, V. Van Speybroeck and P. Van Der Voort, *Microporous Mesoporous Mater.*, 2016, **226**, 110 – 116.
33 J. Lan, D. Cao, W. Wang and B. Smit, *ACS Nano*, 2010, **4**, 4225–4237.
34 V. S. Vyas, F. Haase, L. Stegbauer, G. Savasci, C. Podjaski, F. Ochsenfeld and B. V. Lotsch, *Nat. Commun.*, 2015, **6**, 8508.
35 X. Jiang, P. Wang and J. Zhao, *J. Mater. Chem. A*, 2015, **3**, 7750–7758.
36 L. Stegbauer, K. Schwinghammer and B. V. Lotsch, *Chem. Sci.*, 2014, **5**, 2789–2793.
37 J. Xie, S. A. Shevlin, Q. Ruan, S. J. A. Moniz, Y. Liu, X. Liu, Y. Li, C. C. Lau, Z. X. Guo and J. Tang, *Energy Environ. Sci.*, 2018, **11**, 1617–1624.
38 T. Banerjee and B. V. Lotsch, *Nat. Chem.*, 2018, **10**, 1175–1177.
39 P. Kuhn, M. Antonietti and A. Thomas, *Angew. Chem. International Edition*, 2008, **47**, 3450–3453.
40 S. Hug, M. B. Mesch, H. Oh, N. Popp, M. Hirscher, J. Senker and B. V. Lotsch, *J. Mater. Chem. A*, 2014, **2**, 5928–5936.
41 P. Kuhn, A. Forget, D. Su, A. Thomas and M. Antonietti, *J. Am. Chem. Soc.*, 2008, **130**, 13333–13337.
42 S. Ren, M. J. Bojdys, R. Dawson, A. Laybourn, Y. Z. Khimyak, D. J. Adams and A. I. Cooper, *Adv. Mater.*, 2012, **24**, 2357–2361.
43 S. Tongay, *Applied Physics Reviews*, 2018, **5**, 010401.
44 C. B. Meier, R. S. Sprick, A. Monti, P. Guiglion, J.-S. M. Lee, M. A. Zwijnenburg and A. I. Cooper, *Polymer*, 2017, **126**, 283–290.
45 P. Zhu and V. Meunier, *J. Chem. Phys.*, 2012, **137**, 244703.
46 M. J. Bojdys, J. Jeromenok, A. Thomas and M. Antonietti, *Adv. Mater.*, 2010, **22**, 2202–2205.
47 S. Hug, M. E. Tauchert, S. Li, U. E. Pachmayr and B. V. Lotsch, *J. Mater. Chem.*, 2012, **22**, 13956–13964.
48 C. H. Hendon, J. Bonnefoy, E. A. Quadrelli, J. Canivet, M. B. Chambers, G. Rousse, A. Walsh, M. Fontecave and C. Mellot-Draznieks, *Chem. Eur. J.*, 2016, **22**, 3713–3718.
49 W. A. Maza and A. J. Morris, *J. Phys. Chem. C*, 2014, **118**, 8803–8817.
50 C.-C. Hou, T.-T. Li, S. Cao, Y. Chen and W.-F. Fu, *J. Mater. Chem. A*, 2015, **3**, 10386–10394.
51 D. Yang, S. O. Odoh, T. C. Wang, O. K. Farha, J. T. Hupp, C. J. Cramer, L. Gagliardi and B. C. Gates, *J. Am. Chem. Soc.*, 2015, **137**, 7391–7396.
52 M. Jäger, L. Freitag and L. González, *Coord. Chem. Rev.*, 2015, **304-305**, 146–165.
53 K. Wang, L.-M. Yang, X. Wang, L. Guo, G. Cheng, C. Zhang, S. Jin, B. Tan and A. Cooper, *Angew. Chem. Int. Ed.*, 2017, **56**, 14149–14153.
54 J.-X. Jiang, C. Wang, A. Laybourn, T. Hasell, R. Clowes, Y. Z. Khimyak, J. Xiao, S. J. Higgins, D. J. Adams and A. I. Cooper, *Angew. Chem. Int. Ed.*, 2011, **50**, 1072–1075.
55 G. Kresse and D. Joubert, *Phys. Rev. B*, 1999, **59**, 1758–1775.
56 G. Kresse and J. Hafner, *Phys. Rev. B*, 1993, **47**, 558–561.
57 G. Kresse and J. Hafner, *Phys. Rev. B*, 1994, **49**, 14251–14269.
58 G. Kresse and J. Furthmüller, *Comput. Mat. Sci.*, 1996, **6**, 15–50.
59 G. Kresse and J. Furthmüller, *Phys. Rev. B*, 1996, **54**, 11169–11186.
60 J. P. Perdew, K. Burke and M. Ernzerhof, *Phys. Rev. Lett.*, 1996, **77**, 3865–3868.
61 K. Hendrickx, D. E. P. Vanpoucke, K. Leus, K. Lejaeghere, A. Van Yperen-De Deyne, V. Van Speybroeck, P. Van Der Voort and K. Hemelsoet, *Inorg. Chem.*, 2015, **54**, 10701–10710.

View Article Online
DOI: 10.1039/C9TA00573K

62 J. Heyd, G. E. Scuseria and M. Ernzerhof, *J. Chem. Phys.*, 2003, **118**, 8207–8215.
63 J. Heyd, G. E. Scuseria and M. Ernzerhof, *J. Chem. Phys.*, 2006, **124**, 219906.
64 S.-H. Ke, *Phys. Rev. B*, 2011, **84**, 205415.
65 S. Grimme, J. Antony, S. Ehrlich and H. Krieg, *J. Chem. Phys.*, 2010, **132**, 154104.
66 S. Grimme, S. Ehrlich and L. Goerigk, *J. Comput. Chem.*, 2011, **32**, 1456–1465.
67 K. Lejaeghere, G. Bihlmayer, T. Björkman, P. Blaha, S. Blügel, V. Blum, D. Caliste, I. E. Castelli, S. J. Clark, A. Dal Corso, S. de Gironcoli, T. Deutsch, J. K. Dewhurst, I. Di Marco, C. Draxl, M. Dułak, O. Eriksson, J. A. Flores-Livas, K. F. Garrity, L. Genovese, P. Giannozzi, M. Giantomassi, S. Goedecker, X. Gonze, O. Grånäs, E. K. U. Gross, A. Gulans, F. Gygi, D. R. Hamann, P. J. Hasnip, N. A. W. Holzwarth, D. Iuşan, D. B. Jochym, F. Jollet, D. Jones, G. Kresse, K. Koepernik, E. Küçükbenli, Y. O. Kvashnin, I. L. M. Locht, S. Lubeck, M. Marsman, N. Marzari, U. Nitzsche, L. Nordström, T. Ozaki, L. Paulatto, C. J. Pickard, W. Poelmans, M. I. J. Probert, K. Refson, M. Richter, G.-M. Rignanese, S. Saha, M. Scheffler, M. Schlipf, K. Schwarz, S. Sharma, F. Tavazza, P. Thunström, A. Tkatchenko, M. Torrent, D. Vanderbilt, M. J. van Setten, V. Van Speybroeck, J. M. Wills, J. R. Yates, G.-X. Zhang and S. Cottenier, *Science*, 2016, **351**, 1415–1415.
68 G. Kresse, M. Marsman and J. Furthmüller, *VASP the GUIDE*, Computational Materials Physics, Faculty of Physics, Universität Wien.
69 P. Vinet, J. Ferrante, J. H. Rose and J. R. Smith, *J. Geophys. Res. Solid Earth*, 1987, **92**, 9319–9325.
70 M. Leslie and N. J. Gillan, *J. Phys. C: Solid State Phys.*, 1985, **18**, 973.
71 C. Freysoldt, B. Grabowski, T. Hickel, J. Neugebauer, G. Kresse, A. Janotti and C. G. Van de Walle, *Rev. Mod. Phys.*, 2014, **86**, 253–305.
72 S. Ping Ong, W. Davidson Richards, A. Jain, G. Hautier, M. Kocher, S. Cholia, D. Gunter, V. L. Chevrier, K. A. Persson and G. Ceder, *Comput. Mater. Sci.*, 2013, **68**, 314–319.
73 S. Ling and B. Slater, *J. Phys. Chem. C*, 2015, **119**, 16667–16677.
74 M. A. Nasalevich, M. van der Veen, F. Kapteijn and J. Gascon, *CrystEngComm*, 2014, **16**, 4919–4926.
75 A. Karmakar, A. Kumar, A. K. Chaudhari, P. Samanta, A. V. Desai, R. Krishna and S. K. Ghosh, *Chem. Eur. J*, 2016, **22**, 4931–4937.
76 K. Sakaushi and M. Antonietti, *Acc. Chem. Res.*, 2015, **48**, 1591–1600.

View Article Online
DOI: 10.1039/C9TA00573K

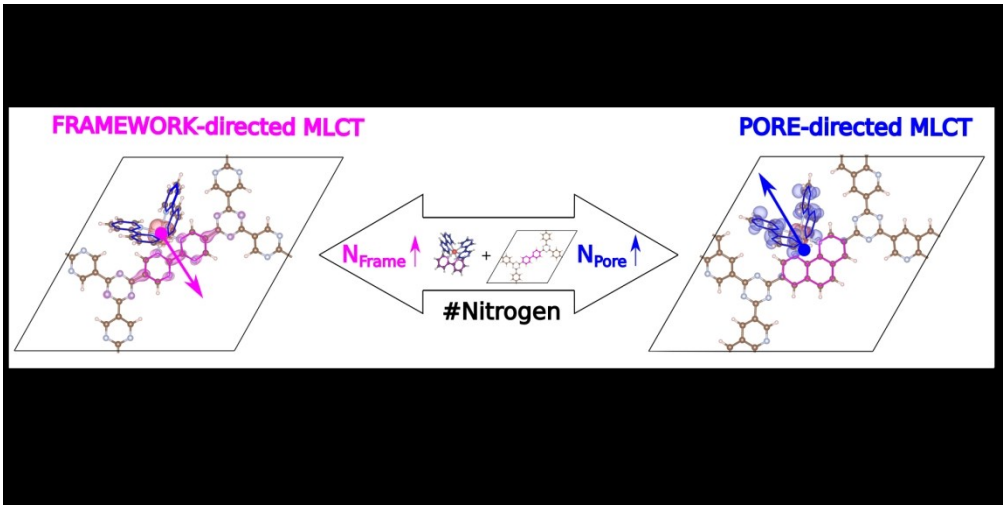

TOC figure : Anchoring Ru(II) polypyridyl complexes onto covalent triazine frameworks yields a versatile photocatalytic system with a charge transfer dependent on the nitrogen content.